

RESEARCH

Open Access



Experimental Study on the Cyclic Performance of Reinforced Concrete Shear Walls Exposed to Fire

Eunmi Ryu¹, Heesun Kim² and Yeongsoo Shin^{3*}

Abstract

The purpose of this study was to investigate the thermal and cyclic behaviors of fire-damaged walls designed with different failure modes, aspect ratios and heated areas. These cyclic behaviors include temperature distribution, maximum lateral load, stiffness, ductility, and energy dissipations, etc. Toward this goal, the concrete wall specimens were exposed to heat following an ISO 834 standard time–temperature curve and the cyclic loading was applied to the fire-damaged walls. The test results showed that exposure to fire significantly reduced the cyclic performance of the RC walls. Especially, it was observed that heated area, designed failure mode, and aspect ratio have influences on maximum lateral loads, stiffness, and ductility of the fire-damaged walls, while almost no effects of the heated area, designed failure mode, and aspect ratio on temperature distribution and energy dissipation were found.

Keywords: reinforced concrete walls, fire, temperature, cyclic test, heated area, failure mode

1 Introduction

Reinforced concrete (RC) wall is a common structural system in Korea, especially for residential buildings. They have a demonstrated high capacity to resist shear forces as well as to prevent the spread of fire. The structural behavior of fire-damaged RC walls is somewhat different than other members such as beams and columns. This is because the RC wall has a relatively large fire exposure surface and the fire-damaged area can vary depending on the fire situation. Crozier and Sanjayan (2000) examined the in-plane load capacity of slender RC walls under fire conditions based on height-to-thickness ratios, cover thicknesses, mix proportions, and loading conditions. Lee and Lee (2013) tested eight RC walls to determine the structural behavior of concrete walls exposed to fire on both surfaces based on wall thickness, concrete

strength, reinforcement ratio, axial load, and curing period. Buchanan and Munukutla (1991) and Zheng and Zhuang (2011) used numerical methods to calculate the load-bearing capacity of fire-damaged RC walls based on boundary conditions, material nonlinearity, load levels, height-to-thickness ratios, material strength, reinforcement ratios, and cover thicknesses. Some researchers (Liu et al. 2010; Xiao et al. 2004) have investigated the effects of axial force, fire exposure, reinforcement ratios, and polypropylene fiber on the cyclic behavior of RC walls under post-fire conditions. Ni and Birely (2018) also developed numerical methods to determine the effect of fire damage on the lateral load resistance of flexure-controlled RC walls. Based on the previous studies of fire-damaged walls, the load capacity of RC walls exposed to fire is reduced significantly for both axial and lateral forces. However, relatively few studies have been conducted on the cyclic performance of RC walls exposed to fire compared to studies about other structural members such as beams and columns (Bratina et al. 2007; El-Hawary et al. 1996; Kodur and Bisby 2005; Kodur and Dwaikat 2008; Lim et al. 2004; Pires et al. 2012; Saafi 2002; Tan and Yao 2003; Tao et al. 2008; Yuan et al. 2010).

*Correspondence: shinys@ewha.ac.kr

³ Full Professor, Dept. of Architectural and Urban Systems Engineering, Ewha Womans University, 52, Ewhayeodae-gil, Seodaemun-gu, Seoul 03760, Republic of Korea

Full list of author information is available at the end of the article
Journal information: ISSN 1976-0485 / eISSN 2234-1315.

In particular, there are insufficient data to understand the cyclic behaviors of fire-damaged RC walls having different fire exposure surface areas and design parameters. Because RC walls in a residential building are commonly used as a partition between compartments, one or less side of wall is likely to be directly exposed to fire. This phenomenon resulted in asymmetry of the fire-damaged wall section, which may further reduce structural performance. In addition, even though the failure modes of non-heated RC walls under cyclic loading can be estimated based on design parameters such as reinforcements and wall dimensions, they have not been clearly defined under conditions when the walls are fully or partially damaged by fire.

Therefore, the purpose of our study was to investigate the effect of heated areas and design parameters on the cyclic behavior of fire-damaged RC walls. Fire and cyclic loading tests were conducted on ten RC walls with varying heated areas and design parameters. Based on the test results, we discuss in this paper temperature distribution, crack patterns, load-bearing capacity, stiffness, ductility, and energy dissipation of the fire-damaged walls according to pre-established test variables.

2 Experimental program

2.1 Test parameters and details of specimens

For the fire and cyclic loading tests, ten specimens with different heated areas, aspect ratios, and designed

failure mode were prepared and are listed in Table 1. Heated areas were the half face and the single of the specimens considering that the heated area of the specimens could be varied according to the type of fire and the floor plan. The aspect ratio (h_w/l_w) is the ratio of wall height to length. Our study used two aspect ratios of 1.5 and 2.5. Therefore, wall lengths varied by 960 mm and 1600 mm for the aspect ratios of 1.5 and 2.5, respectively. The height and thickness of the walls were fixed at 2,400 mm and 200 mm, respectively. In addition, the specimens were reinforced in two ways: (1) LF and QF series walls using reinforcing steel bars of D13 (12.7 mm) only and 2) LS and QS series walls using the increased reinforcement at the wall edges with diameters of D25 (25.4 mm) or D29 (28.6 mm). The ratios of the flexural reinforcing bars (ρ_v) for the specimens LF, QF, LS, QS series were 0.38%, 0.48%, 3.07%, and 1.58%, respectively. Therefore, under non-heated conditions, we expected that the LF and QF series walls were designed to be weak at flexure (flexure yielding mode), while the LS and QS series were designed to be weak at shear (shear failure mode). The ratios of horizontal reinforcing bars (ρ_h) of the specimens with $h_w/l_w = 1.5$ and 2.5 were 0.36% and 0.30%, respectively. A top beam was located on top of the specimens to facilitate the application of the lateral load; a bottom base was also cast to fix the specimens to the laboratory floor. Details of the specimens are shown in Fig. 1a–f.

Table 1 List of specimens.

Specimen	Size (Length x height x thickness) (mm)	Aspect ratio (h_w/l_w)	Failure mode (Flexural reinforcement)	Heated area
LFC	960 × 2400 × 200 (LF)	2.5	Weak at Flexure (D10)	None
LFH1			Weak at Flexure (D10)	Half face
LFH2			Weak at Flexure (D10)	Single face
LSC	960 × 2400 × 200 (LS)	2.5	Weak at Shear (D29-D10)	None
LSH1			Weak at Shear (D29-D10)	Half face
LSH2			Weak at Shear (D29-D10)	Single face
QFC	1600 × 2400 × 200 (QF)	1.5	Weak at Flexure (D10)	None
QFH2			Weak at Flexure (D10)	Single face
QSC	1600 × 2400 × 200 (QS)	1.5	Weak at Shear (D25-D10)	None
QSH2			Weak at Shear (D25-D10)	Single face

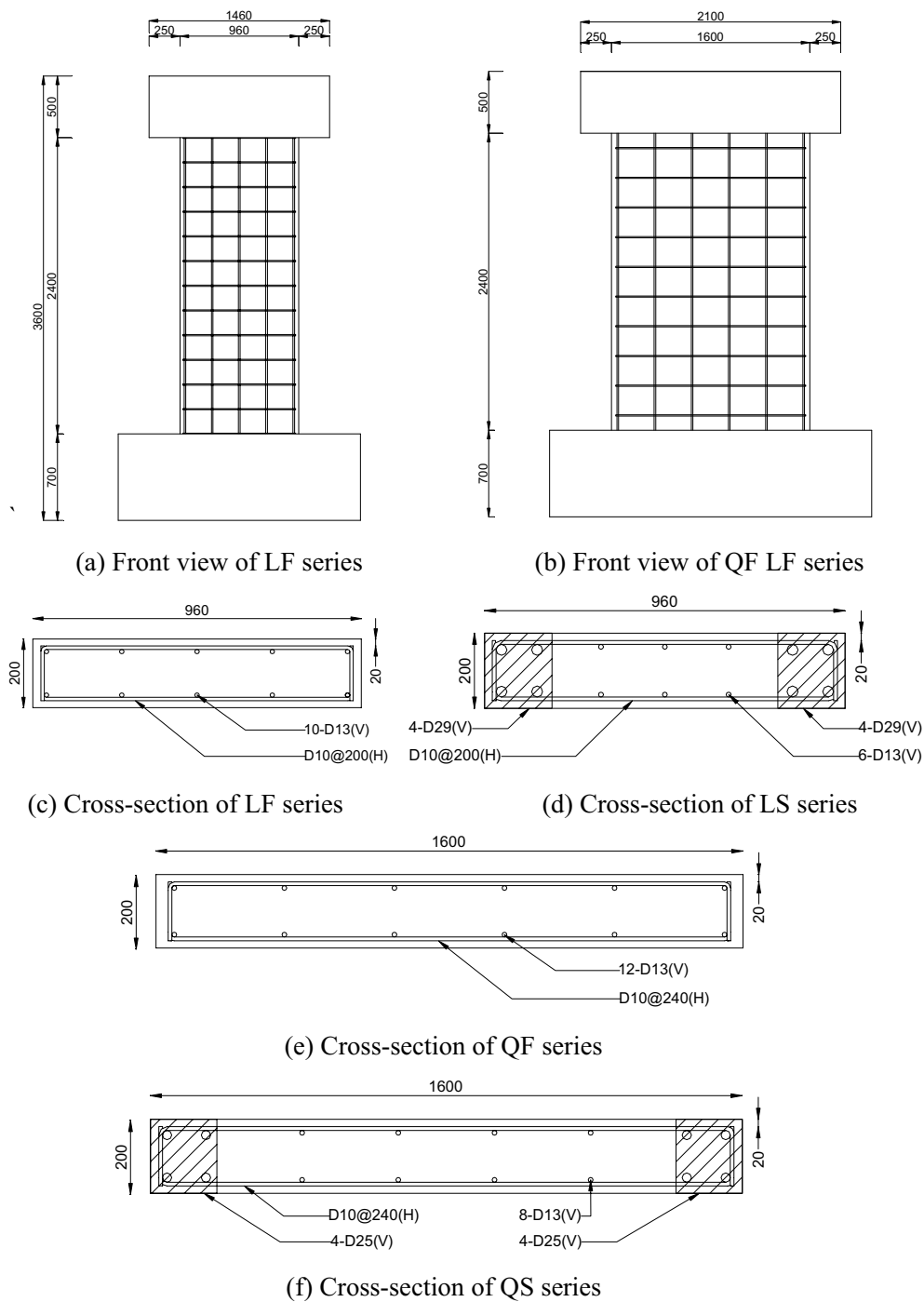


Fig. 1 Geometry and details of specimens (Unit: mm).

2.2 Materials

The proportions of the concrete mix used in the tests are listed in Table 2. A 0.8 kg/m³ of polypropylene fiber was added to the mixture of concrete to prevent spalling during fire tests. After 28 days of curing, strength tests

were performed on the cylinders and the mean compressive and tensile strengths of concrete were obtained as 60.8 MPa and 3.5 MPa, respectively. The yield strength and elastic modulus from the tensile strength tests on the reinforcing bar and stirrup are listed in Table 3.

Table 2 Mixture ratios for concrete.

Design strength (MPa)	28-day compressive strength (MPa)	W/C (%)	Weight per unit volume (kg/m ³)						
			W	C	S	G	FA	Slag	pp fiber
60	60.8	27.9	160	401	715	883	57	115	0.8

W/C Water-to-cement ratio; W Water, C Cement, S Sand, G Gravel, FA Fly ash

2.3 Fire test setup

The specimens were placed in a furnace, as illustrated in Fig. 2. The top beam and bottom base were covered with insulation to avoid exposure to fire. Only one face of the wall specimens was exposed to high temperatures in order to prescribe one directional heating condition. The specimens were heated for two hours in accordance with the ISO 834 standard time–temperature curve (ISO 1999) and not loaded during heating. The furnace temperature was monitored in real time using internal thermocouples. After the fire tests, the walls were cooled at room temperature for one week because the wall temperatures are returned to the room temperature and the residual strength of walls are recovered to the minimum.

Thermocouples were also installed inside the specimens to measure the distribution of temperature during the tests. Thermocouples of specimens heated on the single face were positioned at the centroid of the wall surface area, as illustrated in Fig. 3 (a). For the specimens heated on the half face, thermocouples were positioned on the insulated and non-insulated parts and 10 cm away from the wall center, as illustrated in Fig. 3(b). At each location, four thermocouples were installed along the edge with distances of 20 mm, 40 mm, 100 mm, and 150 mm from the heated surface (Fig. 4).

2.4 Cyclic loading test setup

Figure 4 shows the setup for the cyclic loading test. The walls were subject to a combination of constant axial and cyclic lateral loads. An axial load of $0.1A_c F_{ck}$ (where A_c was the area of the wall cross-section and F_{ck} was the compressive strength of the concrete at ambient temperature) was applied to the top beam of the specimen using a hydraulic jack. The load was maintained during the cyclic loading test. Then, a lateral actuator with a 200 tonf capacity was used to apply a lateral force as shown in the loading history in Fig. 5. The cyclic loading of the specimen was controlled by the horizontal displacement and the same magnitude of displacement was repeated three times. Figure 6 shows the arrangement of the linear variable differential transformers (LVDTs) to measure deformation.

3 Fire Test Results

3.1 Observation After Fire Test

Figure 7 is a photo of the representative heated wall specimen. The wall specimens were heated with laid-down position. In this manner, the wall specimens could be heated in one direction efficiently with other specimens. Even though the laid-down position created bending moment by self-weight, the moment was much less than the nominal moment. After the specimens were heated, they were cooled down in upright position and no lateral deformation was observed. Therefore, almost no lateral deflection was observed from the heated and cooled down specimens. Cracks and discoloration on the surfaces were observed. White stains from the fire exposure surfaces, caused by evaporation of moisture during heating, are visible. No explosive spalling was observed due to the presence of polypropylene fiber. After the fire test, slight deflections were observed on the right but recovered as the walls are cooled. Based on visual observations, there were no noticeable differences in the colors and cracks among the heated specimens.

3.2 Temperature Distribution

The temperatures measured inside the specimens ranged from 90–750 °C, depending on their location. The time–temperature graph of specimen LFH2 in Fig. 8 shows that the temperatures close to the exposure surface increased rapidly until about 20 min after the start of the fire test, while the temperatures close to the unheated side were not increased until 20–30 min of heating due to thermal conductivity. The time–temperature curves of all the tested specimens were similar because heated area and design parameter did not affect temperature distribution of walls.

4 Cyclic Loading Test Results

4.1 Crack Patterns And Failure Mode

Figure 9 shows the damage modes of specimens LFC and LFH2 at drift ratios of 0.35%, 0.60%, 1.25%, and 2.00%. Our discussion is based on the definitions of failure modes and crack patterns suggested by Tang and Su

Table 3 Material properties of steel.

Type	f_y (MPa)	E_s (GPa)
D10	600	194
D13	747	195
D25	542	211
D29	551	204

(2014). In the specimens designed to be weak at flexure, the first horizontal cracking occurred earlier along the edges of heated specimen LFH2 than unheated specimen LFC. At a drift ratio of 0.35% and 0.60% as shown in Fig. 9a, b, e and f, the horizontal cracks propagated to the web of specimen LFC, while diagonal cracks and horizontal cracks appeared in specimen LFH2. As shown in Fig. 9c, d, g and h, the difference in crack patterns between specimens LFC and LFH2 was more obvious at a drift ratio of 1.25% and 2.00%. The fire-damaged specimen LFH2 had more diagonal cracks and the number of cracks increased compared to the unheated specimen LFC. This is because the degradation of concrete due to fire exposure resulted in weakening at shear.

Figure 10 shows the damage modes of specimens LSC and LSH2 at a drift ratio of 0.35%, 0.60%, 1.25%, and 2.00%. In the specimens designed to be weak at shear, the horizontal cracks propagated, forming diagonal cracks. At a drift ratio of 0.35%, 0.60% and 1.25%, it seems that

there were more cracks in the control specimen (LSC) compared to the fire damaged specimen (LSH2). This is because it was not easy to identify the cracks due to loading from those due to fire. Moreover, since specimens LSC and LSH2 were designed to be strong in flexure and weak in shear, cracks of LSH2 would be created mostly by shear and identifiable when the specimen was at near failure. This is why crack density of the specimen LSH2 at a drift ratio of 2.00% had become similar to that of specimen LSC at a drift ratio of 2.00%. Nonetheless, it was clear that the maximum loading bearing capacity and ductility index was smaller in LSH2 compared to LSC. In the case of the specimens LSC and LSH2 at a drift ratio of 2.00%, diagonal cracks spread over the entire wall and the diagonal crack width increased.

Figure 11a–j show the failure crack patterns of specimens at the end of cyclic loading tests. In the specimens designed to be weak at flexure, flexure-tension cracks and flexure-shear cracks were concentrated at the lower part of the specimens (see Fig. 11a–c). Also, concrete crushing and buckling of the vertical rebars occurred in the compression zone. As the specimens were heated, diagonal cracking and concrete cover spalling increased compared to the unheated specimen. In specimen LFH1 that was heated on the half face, concrete cover spalling and flexure-shear cracking were concentrated at the lower part of the exposed surface compared to the surface not exposed. In specimen LFH2 that was heated on the single face, the greater distribution of spalling and flexure-shear

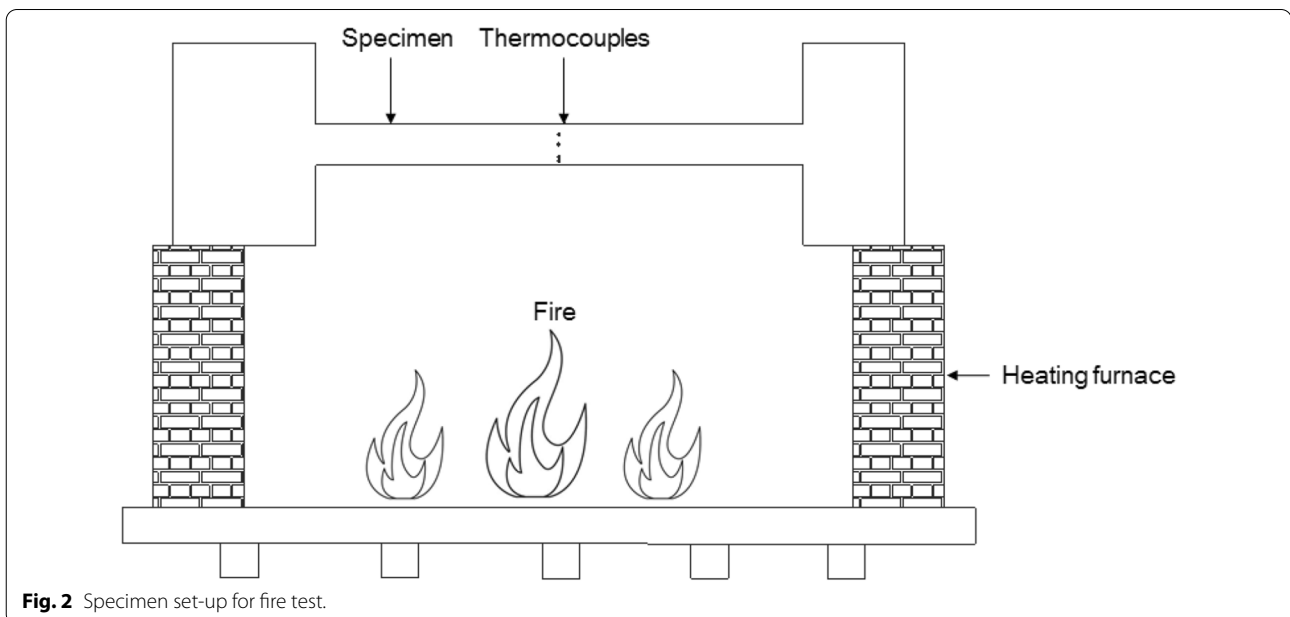
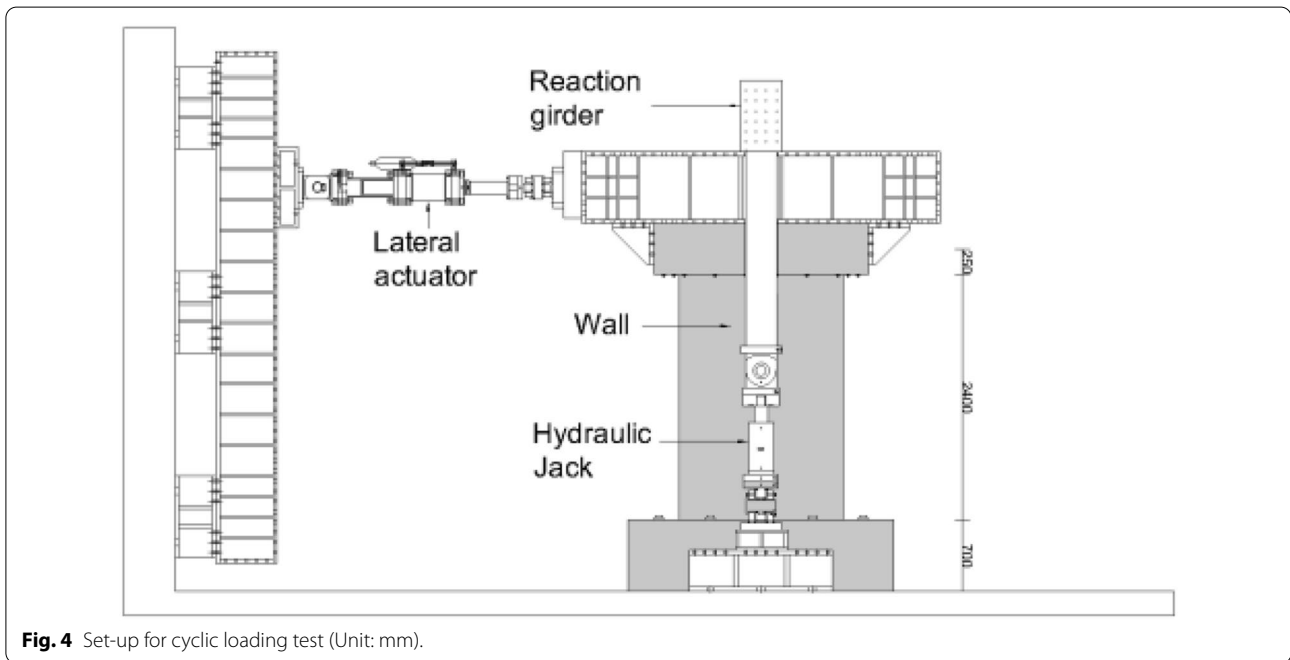
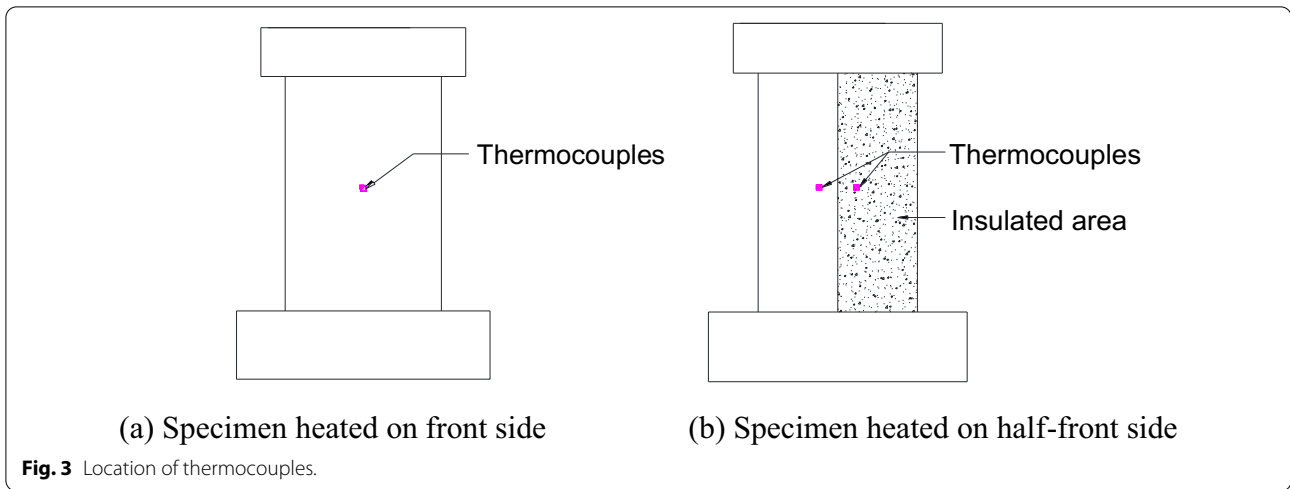


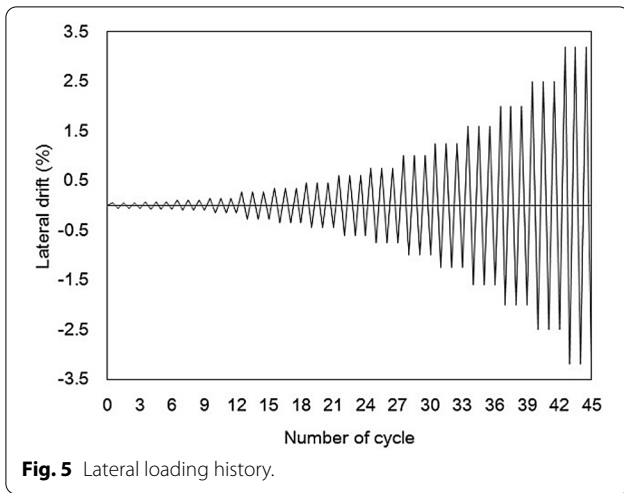
Fig. 2 Specimen set-up for fire test.



cracking developed at the lower part of the specimens compared to specimen LFH1.

Figure 11d–f are photos of the specimens that were designed to be weak at shear. The unheated and heated specimen showed diagonal tension failure. In specimen LSH1 heated on the half face, concrete crushing and buckling of the vertical rebars were observed at the lower

part of the exposed surface and vertical splitting cracks in the surface not exposed. In specimen LSH2 that was heated on the single face, concrete crushing occurred without showing buckling of the vertical rebars. Less vertical splitting cracks occurred in specimen LSH2 than specimen LSH1. The crushing and vertical splitting



cracks in specimens LSH1 may have resulted from asymmetric heating.

There were no noticeable differences in the crack patterns between specimens with $h_w/l_w=2.5$ and 1.5, as shown in Fig. 11g–j. Diagonal cracking and concrete crushing increased compared with specimen QFC. Specimen QSH2 occurred diagonal tension and compression failure but vertical rebars in the boundary zone were not bent unlike specimen LSH2 with $h_w/l_w=2.5$.

4.2 Hysteretic Curves

As illustrated in Fig. 12a–j, the area under hysteresis loops of all heated specimens were thinner than those of unheated specimens. This indicated a reduction in energy dissipation capacity associated with seismic performance. However, the numbers of the hysteretic loops of the heated specimens increased compared with those of the unheated specimens because of decreases in the elasticity of the concrete and steel.

4.3 Maximum Lateral Load

Table 4 lists the maximum lateral loads and corresponding drifts of all specimens. As shown in the first column, the maximum lateral loads of the fire-damaged specimens decreased, but the lateral drift at the maximum lateral load increased because fire exposure caused decreased elastic modulus of concrete and reinforcing bar.

The heated area of the specimens had a considerable influence on the maximum lateral loads of the specimens designed to be weak at flexure, but not specimens designed to be weak at shear. The maximum lateral load of specimens LFH1 and LFH2 were reduced by 5.4% and 9.2% of the control specimen because the heated area of specimen LFH2 was twice the size of that in specimen LFH1. However, even though specimen LSH2 had a heated area twice the area of specimen LSH1, the maximum lateral load of specimens LSH1 and LSH2

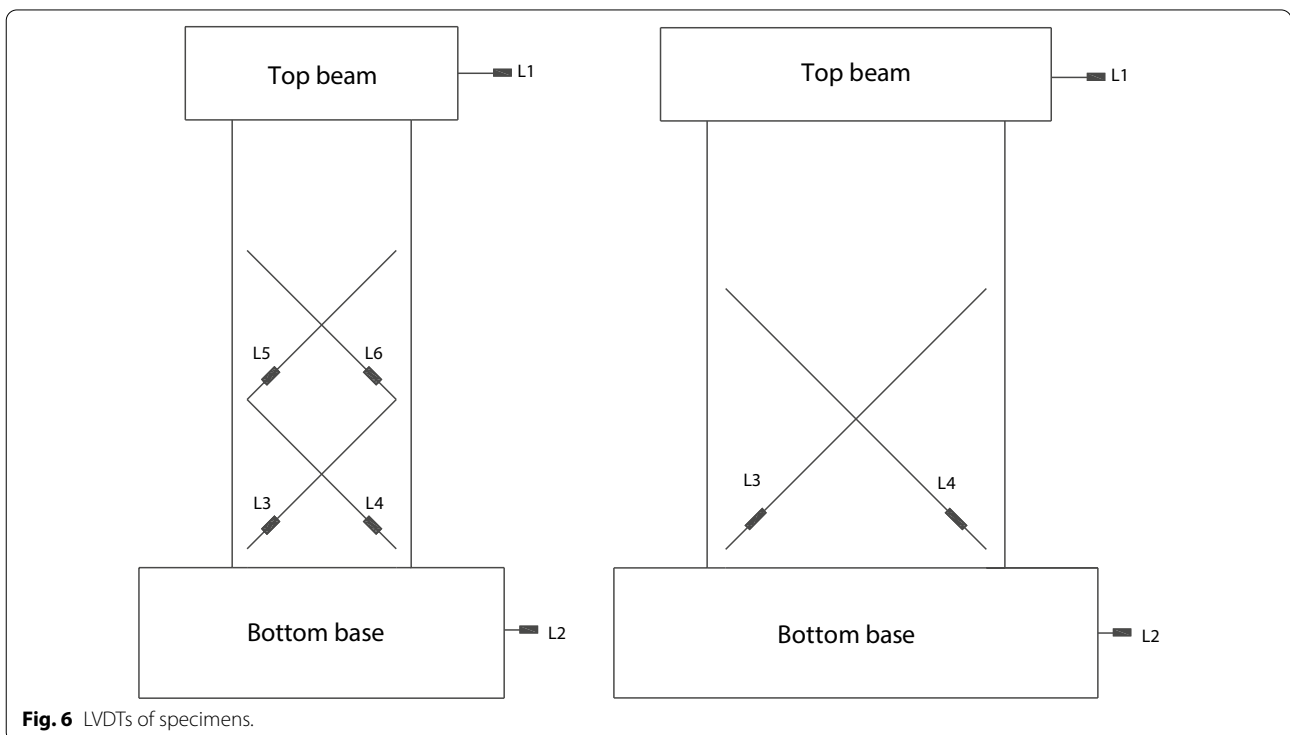




Fig. 7 Specimen QFH2 after the fire test.

specimens designed to be weak at flexure were more vulnerable to fire exposure than specimens designed to be weak at shear.

The maximum lateral loads of the specimens were influenced by the aspect ratio. The reduced rates of the maximum lateral loads in the specimens with $h_w/l_w = 1.5$ were lower than those of in the specimens with $h_w/l_w = 2.5$. The difference in the maximum lateral loads between the reduction rate of the control specimen and specimen QSH2 was the smallest at 1.9%.

The maximum lateral load of the specimens designed to be weak at flexure was more reduced than specimens designed to be weak at shear after the fire tests. To understand this phenomenon, the maximum lateral load was calculated using the numerical method assuming that the compressive strength of concrete was reduced by 25% of the original strength considering the concrete part exposed to temperatures above 500 °C. The maximum lateral loads calculated using the numerical method agreed with those of the experimental results, as shown in Table 5. In the experiments, the maximum lateral loads of the specimens LFH2 and LSH2 were reduced by 9.2% and 4.8%, respectively. The results obtained from the numerical method showed that the maximum lateral loads of specimens LFH2 and LSH2 were reduced by 10.3% and 4.2%, respectively.

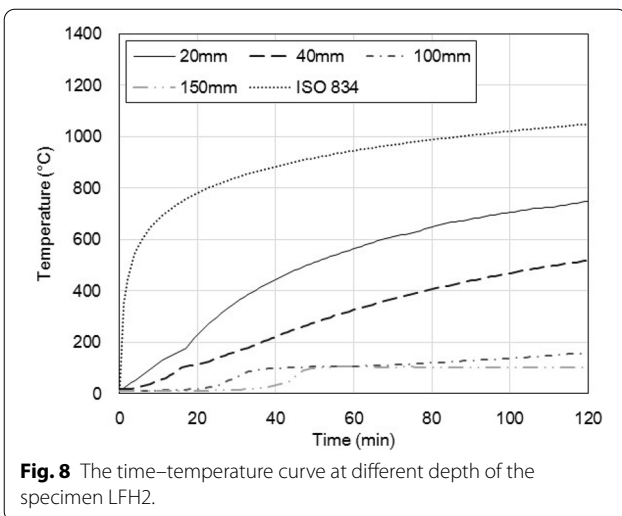


Fig. 8 The time-temperature curve at different depth of the specimen LFH2.

decreased by only 5.5% and 4.8% of the control specimen, respectively. This is because concrete crushing occurred in specimen LSH1, which may fail earlier than specimen LSH2 heated on the single face. In addition, it was obvious that the maximum lateral loads of the

4.4 Stiffness

Since the differences among specimens in maximum lateral loads were small, the stiffness at each loading step was one of the important factors in estimating the cyclic performance of fire-damaged walls. Figure 13 shows stiffness degradation curves of the specimens. Stiffness was the average value of the positive and negative directions except for the specimen heated on the half face. The stiffness of specimens decreased drastically in the early stage of loading and the reduction rate in stiffness decreased slowly as displacement increased. In addition, the difference of stiffness between the heated and unheated specimens decreased as displacement increased.

The stiffness of specimens decreased as the heated area increased. But it could be found that the specimens designed to be weak to flexure are quite vulnerable under partial heating. The stiffnesses of specimens LFH1 and LSH1 heated on the half face were reduced by 33% and 28%, respectively, of the control specimens at a drift ratio of 0.10%. The stiffnesses of specimens LFH2 and LSH2 heated on the single face reduced by 36% at a drift ratio of 0.10%. Even if the heated area of specimen LFH2

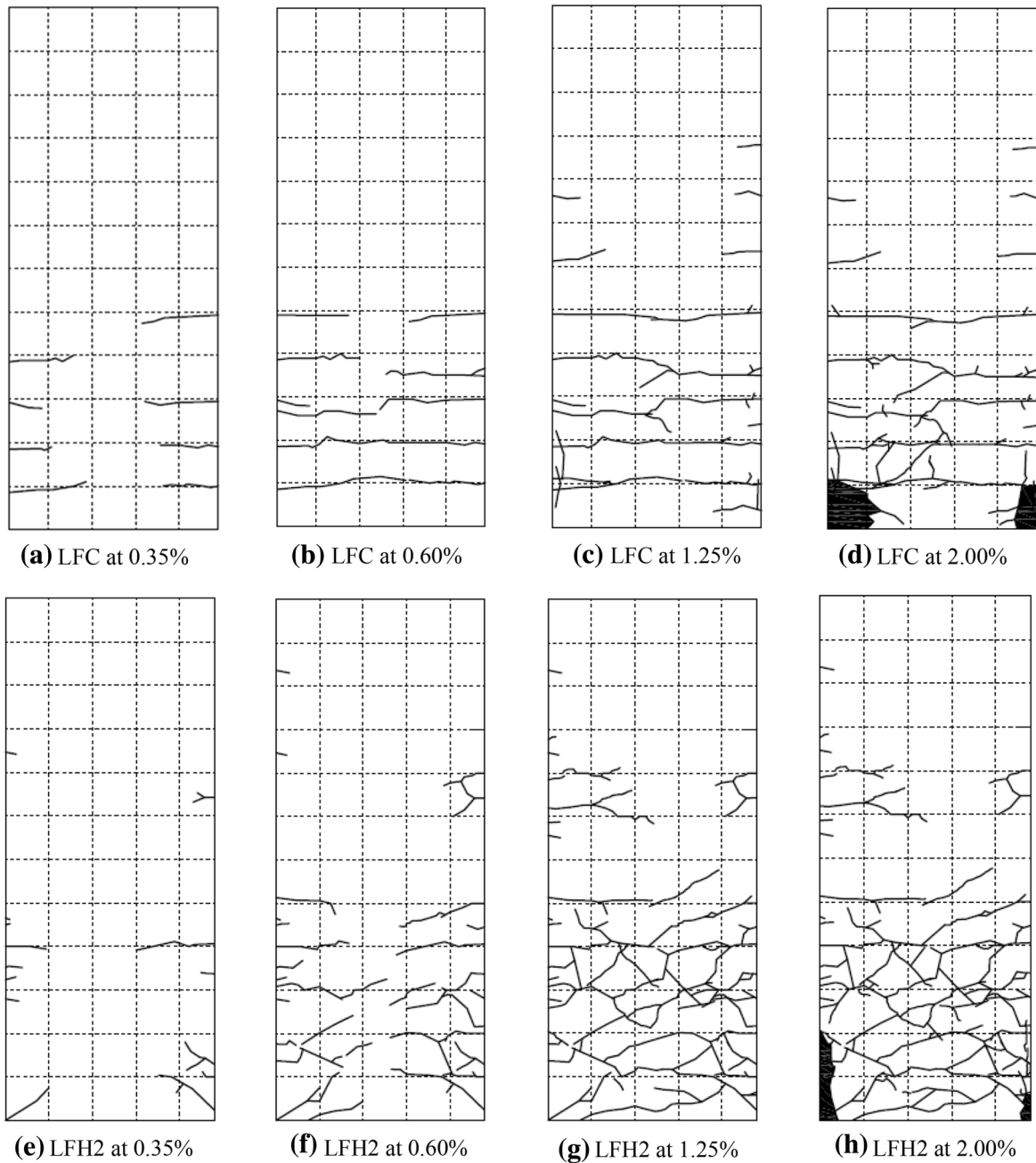


Fig. 9 Damaged modes of specimens LFC and LFH2 at 0.35%, 0.60%, 1.25% and 2.00% drift ratios.

heated on the single face was that of LFH1 heated only on the half face, there was no noticeable difference in the stiffness between the specimens. On the other hand, the stiffness of specimens LSH1 and LSH2 differed by 6% point. In addition, the stiffness of the specimens heated

on the half face differed in the positive and negative loading directions because of the asymmetrically heated area.

In the early stage, the stiffness of specimens designed to be weak at flexure was more reduced than that of specimens designed to be weak at shear due to fire exposure.

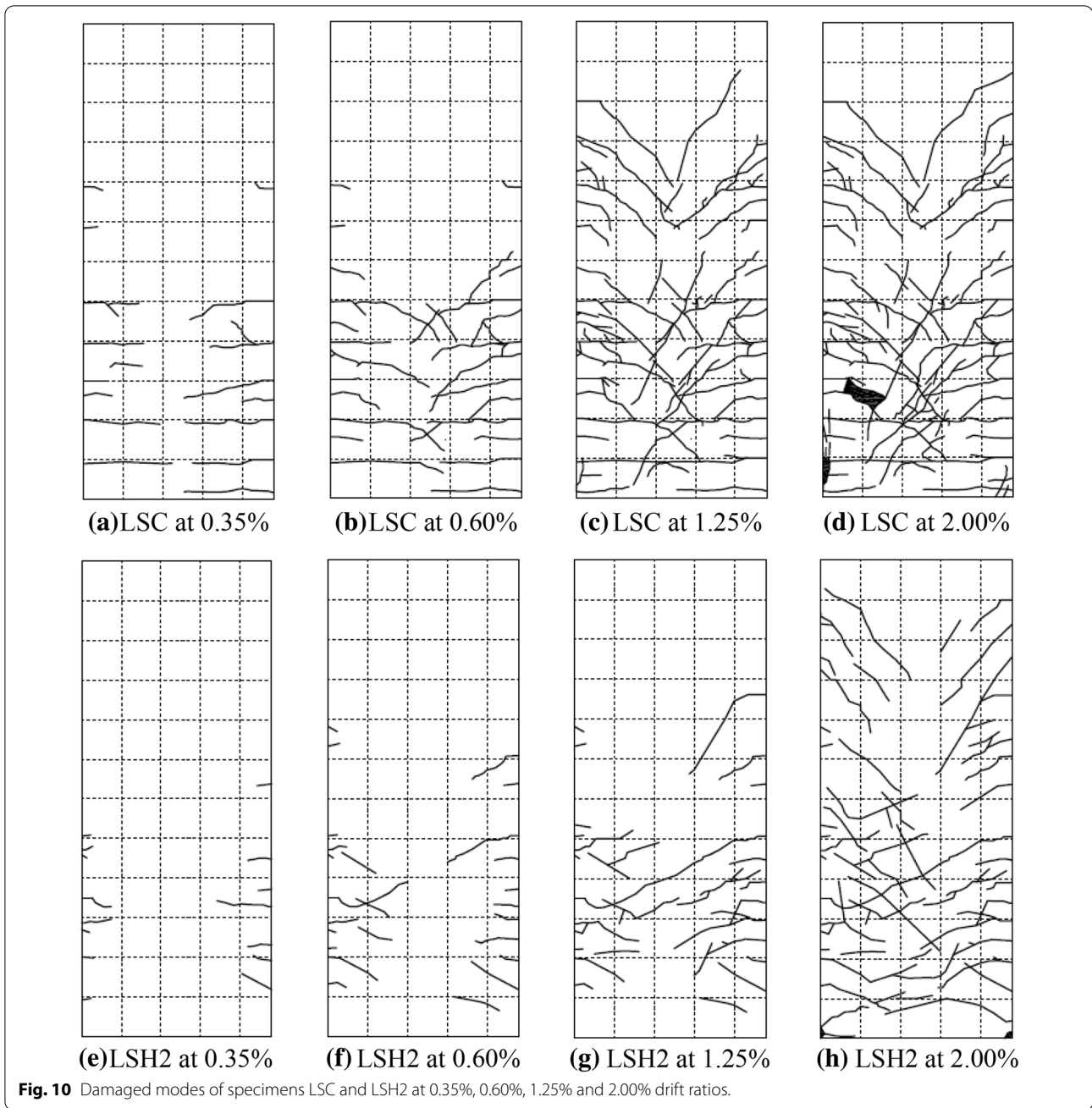


Fig. 10 Damaged modes of specimens LSC and LSH2 at 0.35%, 0.60%, 1.25% and 2.00% drift ratios.

Also, the difference in the reduction rates of stiffness between specimens LFH2 and QFH2 was 10.5% point, while the reduction rates of stiffness between specimens LSH2 and QSH2 were similar. The stiffness of specimen QFH2 with $h_w/l_w = 1.5$ were reduced by 51% of the control specimens at a drift ratio of 0.10%. Therefore, the stiffness of the specimen designed to be weak at flexure was more affected by the aspect ratio than that of the

specimen designed to be weak at shear. It can be said that the wall with low aspect ratio may be more vulnerable in terms of stiffness under a fire.

4.5 The Envelopes Curves

The envelopes for horizontal displacement versus lateral load are shown in Fig. 14. The yield point was determined

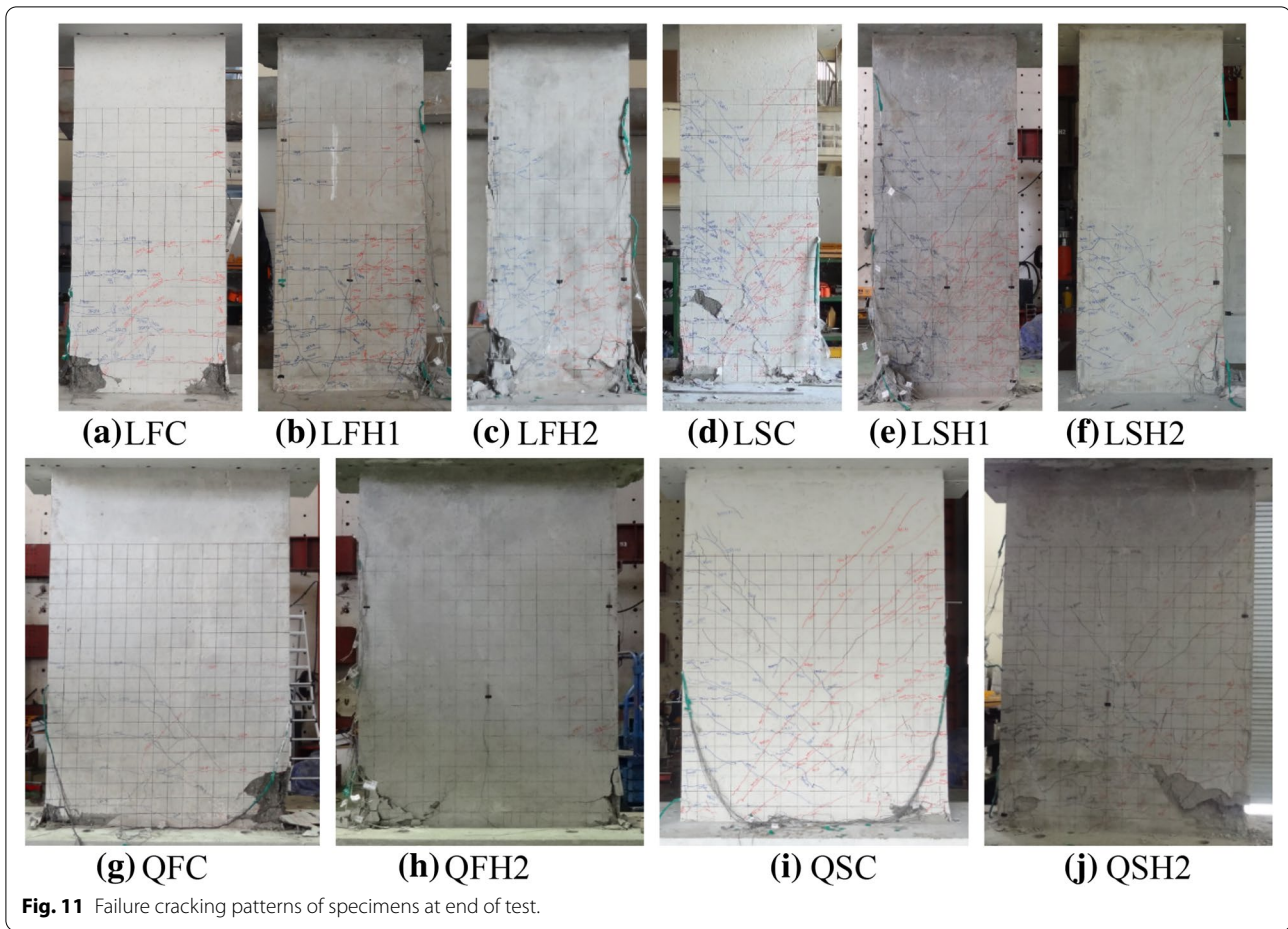


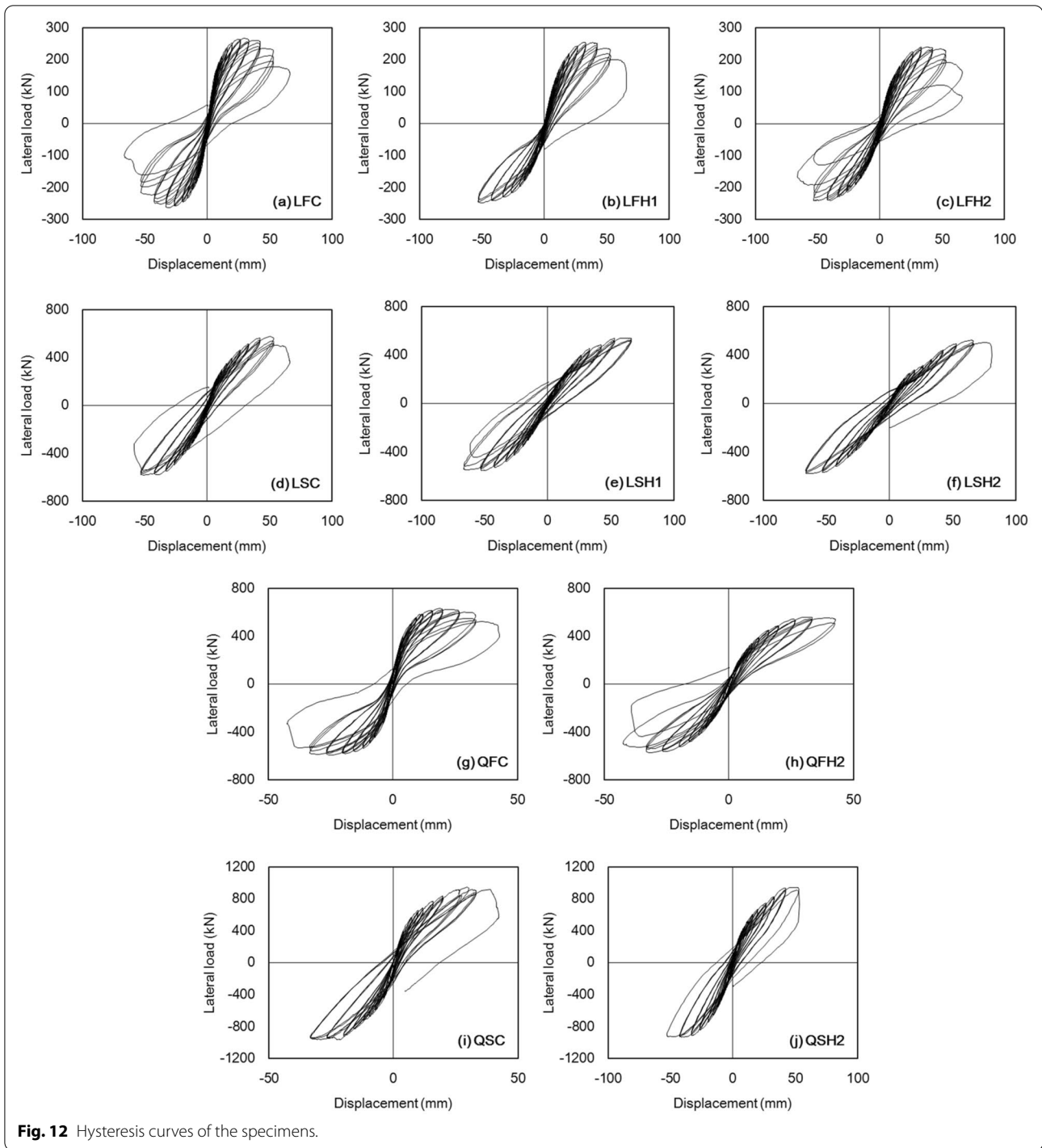
Fig. 11 Failure cracking patterns of specimens at end of test.

in the elastoplastic curve when the areas of A_1 and A_2 obtained from the elastoplastic and actual envelope curves were the same. This was based on the equal energy area method (Nie et al. 2013; Zhang and Wang 2000) as shown in Fig. 15. As shown in Table 6, the yield loads of the heated specimens were smaller than those of the unheated specimens, indicating that exposure to fire had a significant effect on the lateral load of the specimens. However, the displacements of the heated specimens at F_{max} and F_y were greater than those of the unheated specimens due to degradation of elasticity of concrete and reinforcement.

For specimens heated on the half face, the envelope curves in the direction of the exposed side were similar to the curves of the specimens heated on the single face. When the direction of loading was toward the non-exposed side, the envelope curves of the specimens on the half face were greater than those of specimens heated on the single face. This was particularly the case with specimens designed to be weak at shear. Also, the yield

loads and displacements of specimens varied depending on the size of the heating area. The yield load of specimen LFH2 heated on the single face was smaller than that of specimen LFH1 heated on the half face but the difference of yield loads is minimal. On the other hand, the yield load of specimen LSH2 heated on the single face was larger than that of specimen LSH1 heated on the half face even though the heated area of specimen LSH2 was twice the area of that in specimen LSH1. This is because concrete crushing in specimen LSH1 may fail earlier than specimen LSH2 heated on the single face.

The rates of reduction in yield loads of the specimens designed to be weak at flexure were greater than those of the specimens designed to be weak at shear. The rate of reduction for the specimens designed to be weak at flexure was in the range of 9.0%–14.7%. Differences between yield loads of the control specimens and the specimens designed to be weak at shear were significantly small, ranging from 0.9%–3.6%. In the specimens designed



to be weak at flexure, the maximum lateral loads of the heated specimens exhibited a larger displacement than those of the unheated specimens. The specimens

designed to be weak at shear failed immediately upon reaching the maximum loads. The yield displacements of the specimens designed to be weak at flexure were greater than those of the specimens designed to be weak

Table 4 Cyclic loading test results of the specimens.

Specimen	F_{max+} (kN)	F_{max-} (kN)	$F_{max, avg}$ (kN)	Drift at F_{max} (%)
LFC	267.9	-263.1	265.5	+ 1.25/- 1.25
LFH1	254.6	-247.6	251.2	+ 1.25/- 2.00
LFH2	240.6	-241.38	241.0	+ 1.60/- 2.00
LSC	576.6	-579.4	578.0	+ 2.00/- 2.00
LSH1	552.2	-540.5	546.3	+ 2.00/- 2.50
LSH2	522.4	-577.9	550.2	+ 2.50/- 2.50
QFC	632.61	-591.3	611.9	+ 0.75/1.00
QFH2	560.6	-571.7	566.2	+ 1.25/- 1.25
QSC	946.9	-964.6	955.8	+ 1.00/- 1.00
QSH2	945.9	-929.3	937.6	+ 1.60/- 1.60

F_{max+} = the maximum lateral loads of positive directions; F_{max-} = the maximum lateral loads of negative directions; $F_{max, avg}$ = averaged value of F_{max+} and F_{max-} .

Table 5 Comparison of experimental and theoretical values of maximum lateral loads.

Specimen	$F_{max, exp}$ (kN)	Reduction rate of $F_{max, exp}$	F_{theory} (kN)	Reduction rate of F_{theory}
LFC	265.475	1.000	232.64	1.000
LFH2	240.98	0.908	208.72	0.897
LSC	578.025	1.000	499.42	1.000
LSH2	550.15	0.952	472.15	0.956

$F_{max, exp} = F_{max, avg}$; F_{theory} = the calculated maximum lateral loads of the specimens

at shear. The yield loads in the specimens with $h_w/l_w = 2.5$ experienced a greater reduction than those of the specimens with $h_w/l_w = 1.5$. However, the yield displacements of the walls with $h_w/l_w = 2.5$ were smaller than those of walls with $h_w/l_w = 1.5$.

4.6 Ductility

As concrete becomes damaged by fire, a concrete structure tends to become more brittle. Therefore, the ductility index of the tested specimens was calculated based on Eq. (1) (Go et al. 2012).

$\mu = \delta_u / \delta_y$ Eq. (1). where, μ is the ductility index, δ_u is the lateral displacement at maximum load, and δ_y is the lateral displacement at the yield load.

As shown in Table 6, the ductility indices of the heated specimens decreased, although displacements of the heated specimens at failure increased. Also, the results showed that the size of the heated area did not affect the ductility indices of the heated specimens. Even though specimen heated on the single face has twice larger heated area than specimen heated on half face, the difference in ductility indices between specimens having different heated areas was so small that the largest difference in reduction rates was 2.8% point. However, the difference in the ductility index depended on design parameters. The ductility indices of the specimen designed to be weak at flexure exhibited a greater reduction due to fire than those of specimens designed to be weak at shear. Furthermore, the rate of reduction in ductility index increased as the aspect ratio (h_w/l_w) decreased. The ductility indices of specimens QFH2 and QSH2 with $h_w/l_w = 1.5$ were 52% and 78%, respectively, of the control specimens. This was less than those specimens with $h_w/l_w = 2.5$.

4.7 Energy Dissipation

Energy dissipation is defined as the accumulated area enclosed by hysteretic loops for each loading step and can be used to quantify the ability of the tested specimens to absorb seismic energy. Figure 16a–d show the cumulative energy dissipation of in the lateral displacement of the specimens. It is common for the energy dissipation capacity of the heated specimen to decrease because the hysteretic loops become thin and the maximum lateral load is reduced due to exposure to fire.

Comparing specimens LFH1 with LFH2 designed to be weak at flexure, the rate of reduction in cumulative energy dissipation was similar despite the difference in heated areas. On the other hand, the rates of reduction in cumulative energy dissipation of specimens LSH1 and LSH2 were 15% and 25%, respectively, at a drift ratio of 2.00%.

The results also indicated that the design parameters did not affect the cumulative energy dissipation of the heated specimens. The cumulative energy dissipation of all heated specimens was reduced by about 25% at each loading step compared to the control specimens. The cumulative energy dissipation of specimens with $h_w/l_w = 2.5$ and 1.5 is similar because the specimen with $h_w/l_w = 1.5$ had lower stiffness and larger maximum lateral load than specimen with $h_w/l_w = 2.5$.

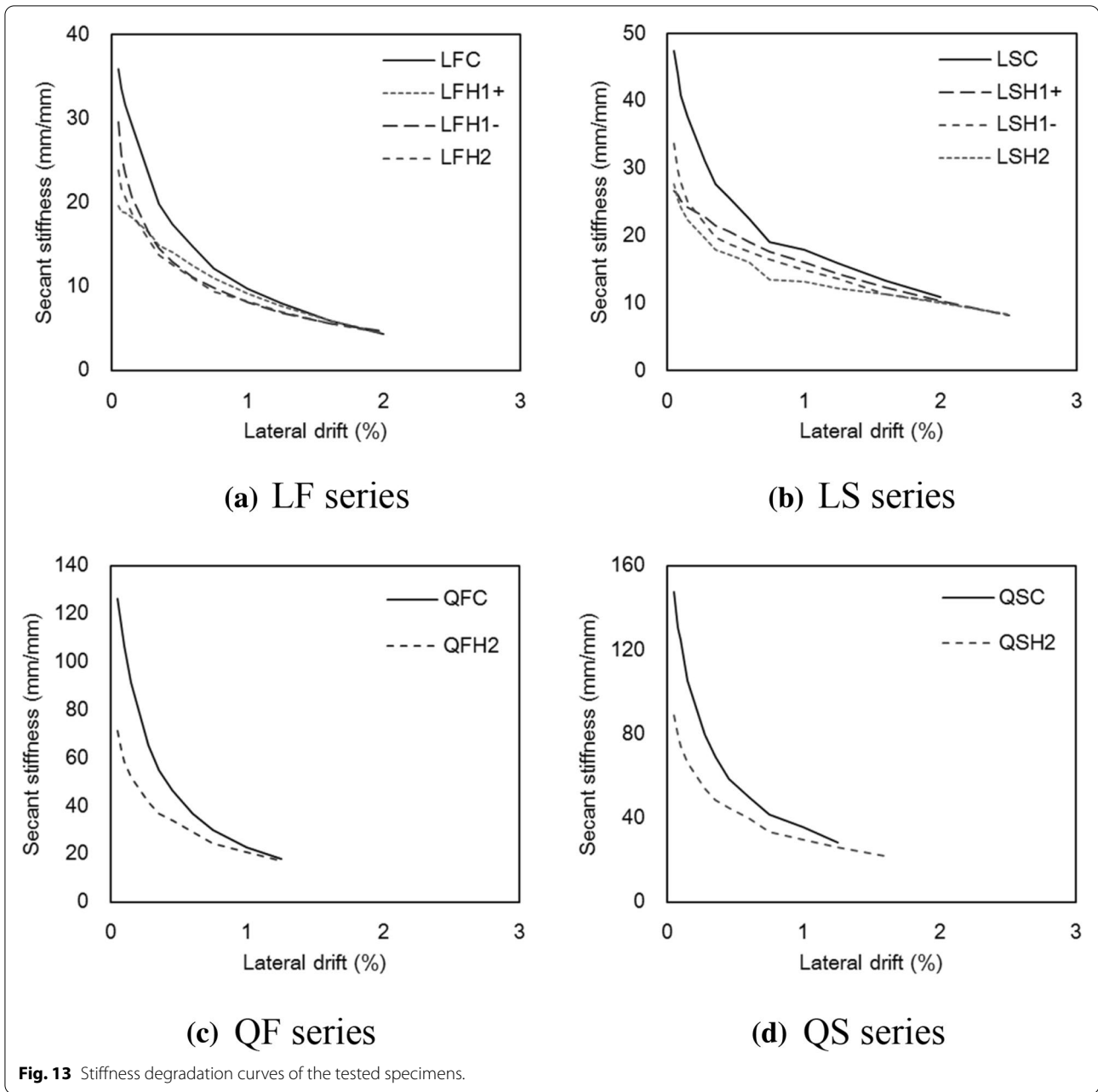
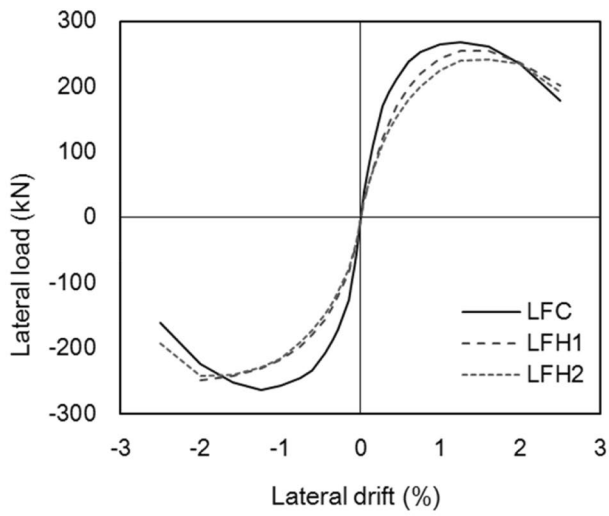
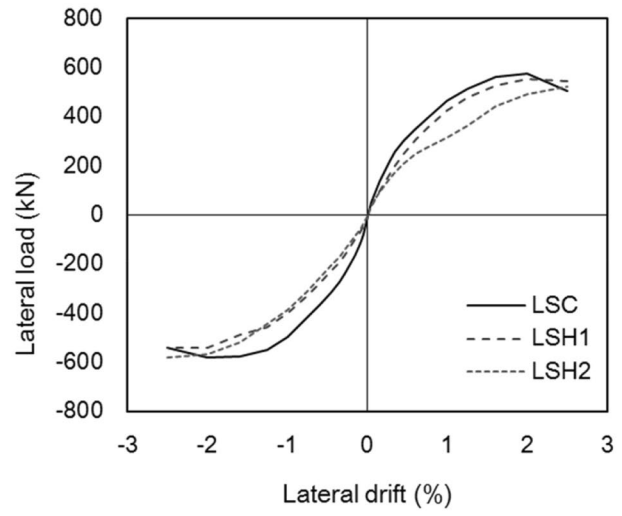


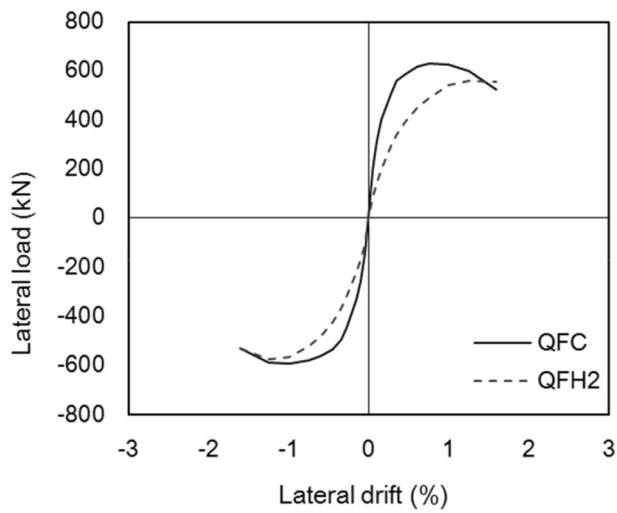
Fig. 13 Stiffness degradation curves of the tested specimens.



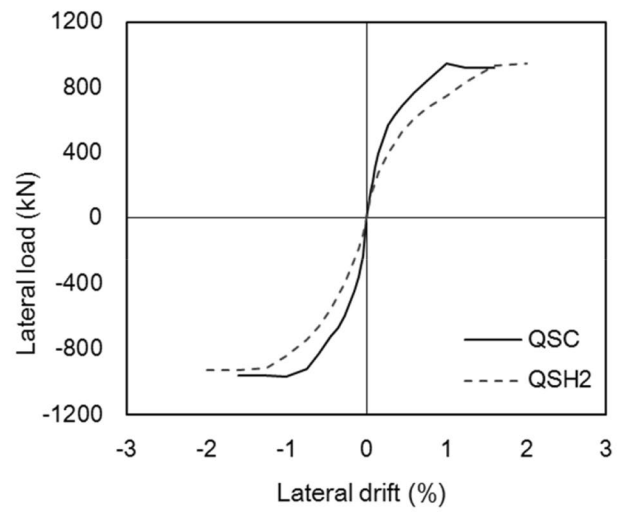
(a) LF series



(b) LS series



(c) QF series



(d) QS series

Fig. 14 Envelope curves of the specimens.

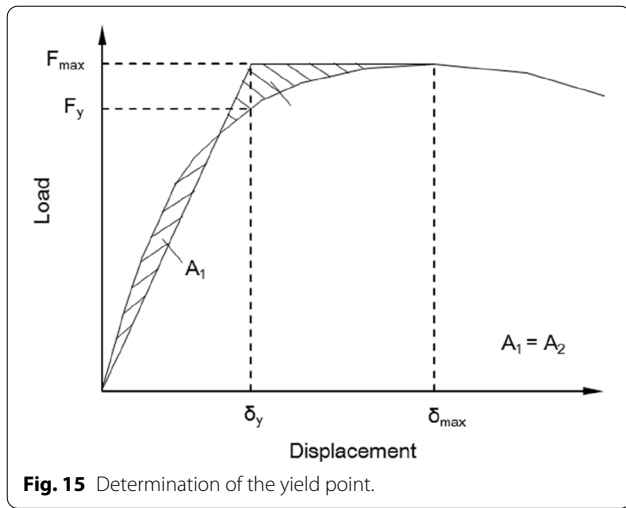


Fig. 15 Determination of the yield point.

Table 6 Yield load, ductility index and displacement obtained from the test.

Specimen	F_y (kN)	δ_y (mm)	δ_u (mm)	Ductility index, μ
LFC	231	14.7	53.0	3.6
LFH1	204	21.2	53.0	2.5
LFH2	197	22.3	53.0	2.4
LSC	495	28.8	53.0	1.8
LSH1	477	35.6	53.0	1.5
LSH2	485	43.3	66.3	1.5
QFC	525	9.2	33.1	3.6
QFH2	478	17.8	33.1	1.9
QSC	797	15.8	33.1	2.1
QSH2	790	26.0	42.4	1.6

F_y = the average yield load; δ_y = the displacement at yield load; δ_u = the displacement at the final cycle step under successive cyclic loadings

5 Conclusions

In our study, the effect of the heated area and design parameters on the cyclic behaviors of RC walls exposed to fire were investigated. The following conclusions were drawn from the results.

- (1) More concrete cover spalling and buckling of rebar occurred in fire-damaged specimens after cyclic loading compared to the unheated specimens. In the specimens designed to be weak at flexure, diagonal cracks and horizontal cracks formed in a web on the heated specimen compared to the unheated specimens.
- (2) Based on cyclic loading tests of the fire-damaged specimens, the maximum lateral loads of the fire-damaged specimens decreased and the displacements under maximum lateral loading increased. This was because exposure to fire resulted in decreased elastic modulus of the concrete and reinforcing bars.
- (3) Even if the heated area of specimen LFH2 heated on the single face was twice that of LFH1 heated only on the half face, the structural behaviors of specimens LFH1 and LFH2 was significantly similar. Also, when the aspect ratio is low, the heated specimens designed to be weak at flexure was more vulnerable to the stiffness and ductility, but not energy dissipation, than the specimen designed to be weak at shear.
- (4) The performance of walls designed to be weak at flexure is reduced significantly under partial heating. In addition, the longer the wall length is, the greater the reduction in performance of fire-damaged wall will occur.

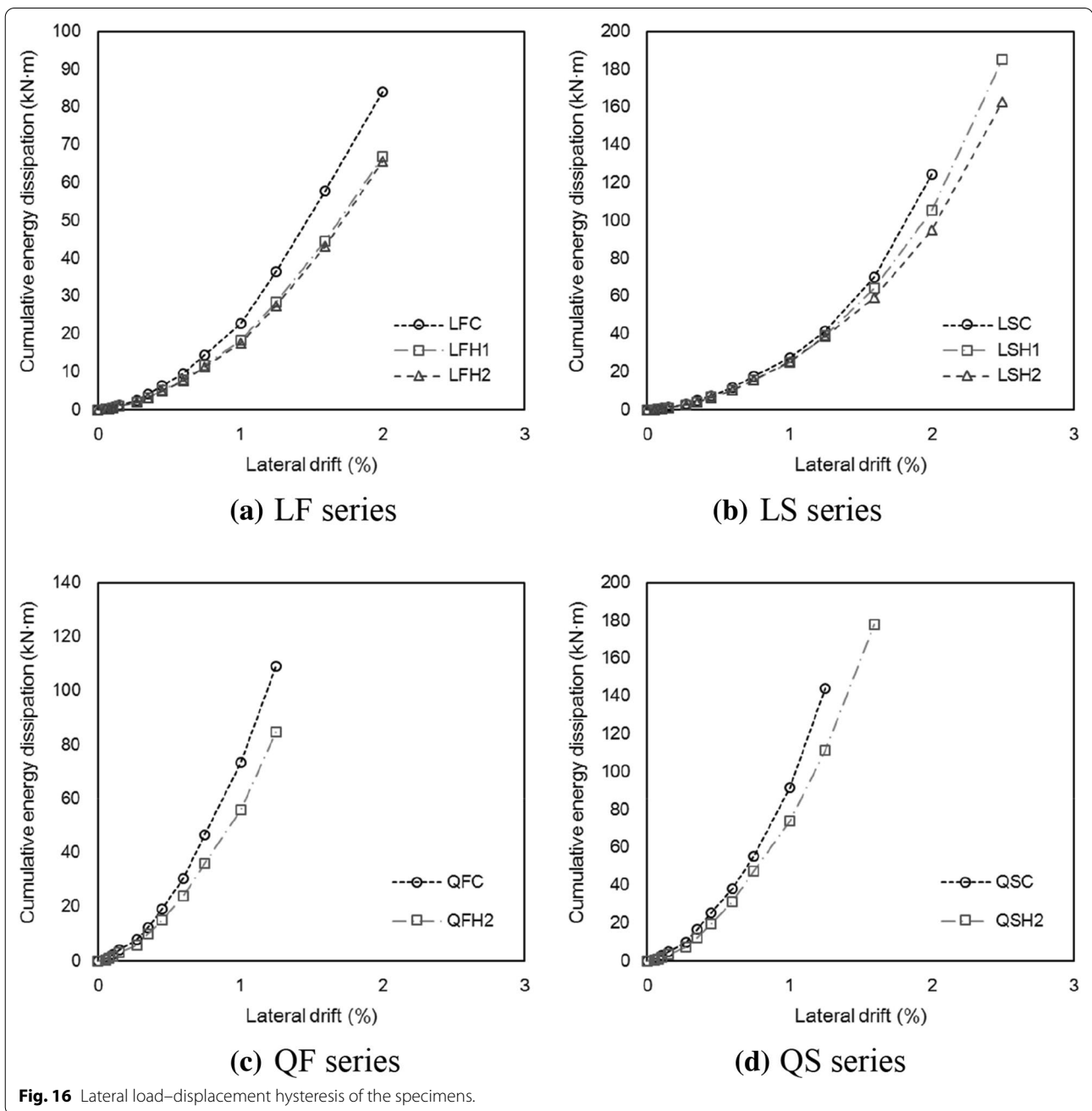


Fig. 16 Lateral load–displacement hysteresis of the specimens.

Authors' information

Eunmi Ryu is a researcher in Fire Research Institute at Korea Institute of Civil Engineering and Building. Heesun Kim is an Associate Professor in Dept. of Architectural and Urban Systems Engineering at Ewha Womans University. Yeongsoo Shin is a Full Professor in Dept. of Architectural and Urban Systems Engineering at Ewha Womans University.

Acknowledgments

Not applicable.

Authors' contributions

All authors contribute equally to this paper. Especially, ER conducted tests and wrote the manuscript. HK participated in analysis of the results and reviewed

the entire manuscript. YS planned test method and variables. All authors read and approved the final manuscript.

Funding

This work was supported by a grant from Urban Architecture Research Program funded by the Ministry of Land, Infrastructure and Transport of Korean government [20AUDP-B100356-06]. This work was supported by a National Research Foundation of Korea (NRF) grant funded by the Korea government (MSIT) [NRF-2017R1A2B4009072].

Availability of data and materials

The data and materials had been included in the manuscript.

Competing interests

The authors declare that they have no competing interests.

Author details

¹ Researcher, Fire Research Institute, Korea, Institute of Civil Engineering and Building Technology, 283, Goyang-daero, Ilsanseo-gu, Goyang-si, Gyeonggi-do 10223, Republic of Korea. ² Associate Professor, Dept. of Architectural and Urban Systems Engineering, Ewha Womans University, 52, Ewhayeo-dae-gil, Seodaemun-gu, Seoul 03760, Republic of Korea. ³ Full Professor, Dept. of Architectural and Urban Systems Engineering, Ewha Womans University, 52, Ewhayeo-dae-gil, Seodaemun-gu, Seoul 03760, Republic of Korea.

Received: 20 July 2020 Accepted: 17 October 2020

Published online: 18 December 2020

References

- Bratina, S., Saje, M., & Planinc, I. (2007). The effects of different strain contributions on the response of RC beams in fire. *Engineering Structures*, 29(3), 418–430.
- Buchanan, A. H., & Munukutla, V. R. (1991). Fire resistance of load-bearing reinforced concrete walls. *Fire Safety Science*, 3, 771–780.
- Crozier, D. A., & Sanjayan, J. G. (2000). Tests of load-bearing slender reinforced concrete walls in fire. *Structural Journal*, 97(2), 243–251.
- El-Hawary, M. M., Ragab, A. M., El-Azim, A. A., & Elibiari, S. (1996). Effect of fire on flexural behaviour of RC beams. *Construction and Building materials*, 10(2), 147–150.
- Go, C., Tang, J., Chi, J., Chen, C., & Huang, Y. (2012). Fire-resistance property of reinforced lightweight aggregate concrete wall. *Construction and Building Materials*, 30, 725–733.
- ISO. (1999). 834: *Fire resistance tests-elements of building construction*. Geneva, Switzerland: International Organization for Standardization.
- Kodur, V., & Bisby, L. A. (2005). Evaluation of fire endurance of concrete slabs reinforced with fiber-reinforced polymer bars. *Journal of structural engineering*, 131(1), 34–43.
- Kodur, V., & Dwaikat, M. (2008). A numerical model for predicting the fire resistance of reinforced concrete beams. *Cement and Concrete Composites*, 30(5), 431–443.
- Lee, S., & Lee, C. (2013). Fire resistance of reinforced concrete bearing walls subjected to all-sided fire exposure. *Materials and structures*, 46(6), 943–957.
- Lim, L., Buchanan, A., Moss, P., & Franssen, J.-M. (2004). Numerical modelling of two-way reinforced concrete slabs in fire. *Engineering structures*, 26(8), 1081–1091.
- Liu, G., Song, Y., & Qu, F. (2010). Post-fire cyclic behavior of reinforced concrete shear walls. *Journal of Central South University of Technology*, 17(5), 1103–1108.
- Ni, S., & Birely, A. C. (2018). Post-fire seismic behavior of reinforced concrete structural walls. *Engineering Structures*, 168, 163–178.
- Nie, J., Hu, H., Fan, J., Tao, M., Li, S., & Liu, F. (2013). Experimental study on seismic behavior of high-strength concrete filled double-steel-plate composite walls. *Journal of Constructional Steel Research*, 88, 206–219.
- Pires, T. A., Rodrigues, J. P. C., & Silva, J. J. R. (2012). Fire resistance of concrete filled circular hollow columns with restrained thermal elongation. *Journal of Constructional Steel Research*, 77, 82–94.
- Saafi, M. (2002). Effect of fire on FRP reinforced concrete members. *Composite Structures*, 58(1), 11–20.
- Tan, K., & Yao, Y. (2003). Fire resistance of four-face heated reinforced concrete columns. *Journal of Structural Engineering*, 129(9), 1220–1229.
- Tang, T. O., & Su, R. K. L. (2014). Shear and flexural stiffnesses of reinforced concrete shear walls subjected to cyclic loading. *The Open Construction and Building Technology Journal*, 8(1).
- Tao, Z., Han, L.-H., & Zhuang, J.-P. (2008). Cyclic performance of fire-damaged concrete-filled steel tubular beam-columns repaired with CFRP wraps. *Journal of Constructional Steel Research*, 64(1), 37–50.
- Xiao, J., Li, J., & Jiang, F. (2004). Research on the seismic behavior of HPC shear walls after fire. *Materials and structures*, 37(8), 506–512.
- Yuan, G., Zhang, X., Zhang, Y., & Zhou, L. (2010). Simplified calculation on bearing capacity of normal section for RC column subjected to fire on four surfaces. *Sichuan Building Science*, 36(04), 91–94.
- Zhang, Y., & Wang, Z. (2000). Seismic behavior of reinforced concrete shear walls subjected to high axial loading. *Structural Journal*, 97(5), 739–750.
- Zheng, Y. Q., & Zhuang, J. P. Analysis on fire resistance of reinforced concrete Wall. *Proc., Advanced Materials Research*, Trans Tech Publ, 797–800.

Publisher's Note

Springer Nature remains neutral with regard to jurisdictional claims in published maps and institutional affiliations.

Submit your manuscript to a SpringerOpen® journal and benefit from:

- Convenient online submission
- Rigorous peer review
- Open access: articles freely available online
- High visibility within the field
- Retaining the copyright to your article

Submit your next manuscript at ► [springeropen.com](https://www.springeropen.com)